



Cite this: *Org. Biomol. Chem.*, 2015, **13**, 8261

Discrimination of the prochiral hydrogens at the C-2 position of *n*-alkanes by the methane/ammonia monooxygenase family proteins†

Akimitsu Miyaji, Teppei Miyoshi, Ken Motokura and Toshihide Baba*

The selectivity of ammonia monooxygenase from *Nitrosomonas europaea* (AMO-Ne) for the oxidation of C₄–C₈ *n*-alkanes to the corresponding alcohol isomers was examined to show the ability of AMO-Ne to recognize the *n*-alkane orientation within the catalytic site. AMO-Ne in whole cells produces 1- and 2-alcohols from C₄–C₈ *n*-alkanes, and the regioselectivity is dependent on the length of the carbon chain. 2-Alcohols produced from C₄–C₇ *n*-alkanes were predominantly either the *R*- or *S*-enantiomers, while 2-octanol produced from *n*-octane was racemic. These results indicate that AMO-Ne can discriminate between the prochiral hydrogens at the C-2 position, with the degree of discrimination varying according to the *n*-alkane. Compared to the particulate methane monooxygenase (pMMO) of *Methylococcus capsulatus* (Bath) and that of *Methylosinus trichosporium* OB3b, AMO-Ne showed a distinct ability to discriminate between the orientation of *n*-butane and *n*-pentane in the catalytic site.

Received 1st April 2015,
Accepted 25th June 2015
DOI: 10.1039/c5ob00640f

www.rsc.org/obc

1. Introduction

The selective oxidation of *n*-alkanes to alcohols is accomplished by several monooxygenases under ambient conditions.¹ For instance, methane monooxygenase produces methanol selectively from methane; the most inert *n*-alkane. A further challenge in the oxidation of *n*-alkanes is the discrimination of a specific C–H bond within the *n*-alkane molecule to selectively produce a specific regioisomer and enantiomer of the corresponding alcohol. For an enzyme to discriminate between multiple C–H bonds in a *n*-alkane molecule, its active site must recognize the orientation of a *n*-alkane molecule in the catalytic site.² Specific interactions, hydrogen bonds and van der Waals interactions between a *n*-alkane and the surface of the active site play a key role in its recognition. Thus, some or all amino acid residues composing the active site of enzymes should affect the regio- and enantioselectivity of the alcohol isomers produced from *n*-alkanes.

The active site of the copper-containing particulate methane monooxygenase of *Methylococcus capsulatus* (Bath) (pMMO-Mc) and *Methylosinus trichosporium* OB3b (pMMO-Mt) can recognize *n*-butane and *n*-pentane. These pMMOs produce (*R*)-2-alcohols selectively from *n*-butane and *n*-pentane,³ indicating that the active site of these monooxygenases is

able to discriminate the pro-*R* hydrogen at C-2 of *n*-butane and *n*-pentane. In addition, the two pMMOs have the same substrate range and product selectivities,^{3,4} suggesting that the two pMMOs have common protein structures around the catalytic site, which involve the recognition of *n*-butane and *n*-pentane. However, the amino acid sequences and the crystal structures of pMMO-Mc and pMMO-Mt show some structural differences between the active sites, although the shapes of overall protein are almost identical.⁵ Therefore, the amino acid residues in the active site controlling the orientation of *n*-butane and *n*-pentane are possibly conserved in the two pMMOs, and differences in the local structure of the active site do not affect the orientation of *n*-butane and *n*-pentane.

The location of the pMMO catalytic site is a controversial issue. Based on the crystal structure of pMMO, three metal sites are proposed as the catalytic site of pMMO: di-copper center,⁶ mono-copper center,⁷ and tri-copper center.⁸ A putative substrate binding cavity is adjacent to each copper center.^{3b,9} However, the di-copper center is most likely the catalytic site because the recombinant protein of pMMO subdomain containing only the di-copper center shows activity toward methane oxidation to methanol.⁶ In addition, the chemistry of various model copper complexes and DFT calculations of the di-copper center of the pMMO active site led to the proposal that a mixed-valent (μ-oxo) (μ-hydroxo) Cu^{II}Cu^{III} species catalyzes the homolytic cleavage of the C–H bond in methane.¹⁰ Furthermore, the C–H bond cleavage and C–O bond formation proceed with retention of configuration for *n*-alkanes.¹¹

Department of Environmental Chemistry and Engineering, Tokyo Institute of Technology, 4259 G-1-14 Nagatsuta-cho, Midori-ku, Yokohama 226-8502, Japan.
E-mail: tbaba@chemenv.titech.ac.jp; Fax: +81-45-924-5441; Tel: +81-45-924-5480
†Electronic supplementary information (ESI) available. See DOI: 10.1039/c5ob00640f

For determination of the amino acid residue(s) involved in substrate recognition, site-directed mutagenesis is the most effective technique. However, this genetic engineering procedure cannot be applied to the study of pMMO, because the heterologous gene expression system of pMMO is not established. Alternatively, by comparing the protein structures and enzyme functions among the family proteins, the key amino acid residue(s) involved in the molecular recognition can be predicted.

In this study, we focused on the ammonia monooxygenase of *Nitrosomonas europaea* (AMO-Ne) as a family protein of pMMO-Mc and pMMO-Mt. AMO-Ne plays a role in the physiological oxidation of ammonia to hydroxylamine,¹² which is different physiological role to pMMO. Crystal structure of AMO-Ne has not been revealed. However, the high amino acid sequence homology between AMO-Ne and the two pMMOs (approximately 40% identity and 65% similarity)¹³ suggests that these enzymes are evolutionarily related each other, and indicates that the tertiary and quaternary protein structures of these enzymes have high similarity. In addition, the amino acid residues composing the metal binding site in the two pMMOs are well conserved in AMO-Ne, which suggests that AMO-Ne has the same catalytic site as the two pMMOs. In fact, AMO-Ne oxidizes some *n*-alkanes including methane as non-growth substrates to the corresponding alcohols.^{14a}

On the other hand, the substrate binding site of AMO-Ne may be larger than that of the two pMMOs based on the larger substrate range of AMO-Ne.¹⁴ In addition, differences in the structure of the substrate binding site of AMO-Ne compared to the two pMMOs is suggested by the difference in regioselectivity of AMO-Ne for alcohols from alkanes,^{14b} and its enantioselectivity for epoxides from alkenes.¹⁵ The difference in the local structure of these enzymes may also affect their ability to discriminate between the prochiral C-H bonds at the C-2 position of *n*-alkanes, which enables the enzyme to selectively generate a specific enantiomer of 2-alcohols. Further, AMO-Ne may be proper enzyme for predicting the key amino acid residue(s) involved in the molecular recognition of *n*-alkane in pMMO/AMO family proteins through the comparison of their protein structures.

We report here the influence of the protein structure of copper-containing monooxygenases on their ability to recognize *n*-alkanes. We investigated the selectivity for 2-alcohol enantiomers produced by the oxidation of C₄–C₈ *n*-alkanes using the whole cells of AMO-Ne. In addition, we constructed a homology protein structure model of the substrate binding cavity in AMO-Ne based on the protein structure of pMMO-Mc. According to the product selectivity and the spatial structure of the substrate binding cavity, the orientation of the *n*-alkanes in the substrate binding cavity of AMO-Ne was estimated. Furthermore, comparing the *n*-alkane orientations and the spatial structure of the substrate binding cavity, we discussed the amino acid residue(s) affecting the regio- and enantioselectivities of *n*-alkane oxidation to the corresponding alcohol by pMMO/AMO family proteins.

2. Results and discussion

2.1 *n*-Butane and *n*-pentane oxidation by AMO-Ne

Both 1-butanol and 2-butanol were produced from the oxidation of *n*-butane by AMO-Ne in whole cells, as reported in ref. 14a. As shown in Fig. 1, butanols were produced at a constant rate for about 15 min after the reaction started, and the production rate decreased gradually. Butyraldehyde and 2-butanone, which can be produced by further oxidation of butanols, were not observed in the reaction. We further confirmed that no butanols consumption was observed when the whole cells of AM-Ne were incubated with butanols. These results indicate that the whole cells of AMO-Ne specifically show activity toward *n*-butane oxidation to butanols.

In the initial stage of *n*-butane oxidation, 82% of the product was 2-butanol; the distribution of butanol regioisomers was almost constant during the reaction, as shown in Fig. 1. These results indicate that AMO-Ne in whole cells produces 2-butanol selectively from *n*-butane. In other words, *n*-butane oxidation proceeds predominantly when the C-2 position of *n*-butane is located close to the catalytic site of AMO-Ne. Further, we investigated the selectivity for 2-butanol enantiomers from *n*-butane. Of the 2-butanol produced, 77% was the *S*-enantiomer, as shown in Table 1; the enantioselectivity was also almost constant during the reaction. Thus, AMO-Ne shows some selectivity for (*S*)-2-butanol in *n*-butane oxidation. The selectivity indicates that the pro-*S* hydrogen at the C-2 position of *n*-butane is preferably oriented toward the catalytic site within AMO-Ne.

For the *n*-pentane oxidation by AMO-Ne, both 1-pentanol and 2-pentanol were produced (Fig. S1(A) in ESI†) as reported in ref. 14a; 3-pentanol and other oxidation products such as ketone and aldehyde were not observed. The selective pro-

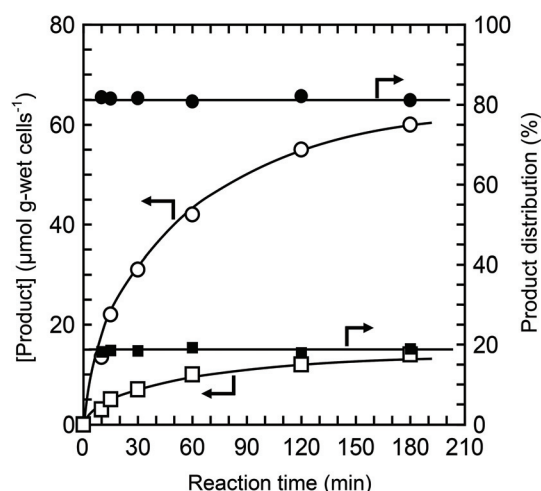


Fig. 1 Butanol production in *n*-butane oxidation by AMO-Ne. ○, ●: 2-butanol; □, ■: 1-butanol. Arrows indicate axis of data. The reaction was carried out at 30 °C in 50 mM phosphate buffer (pH 7.0) containing 1.2 mM duroquinol, and 4.5 g-wet cells per L whole cells. The initial concentration of *n*-butane (dissolved) was 230 μM.

Table 1 Comparison of the selectivity for 2-alcohol enantiomers in *n*-butane and *n*-pentane oxidation among AMO-Ne, pMMO-Mt, and pMMO-Mc

Biocatalyst	Amount of 2-alcohol ^a ($\mu\text{mol g-wet per cells}$)	Distribution of 2-alcohol enantiomers (%)		ee ^c (%)
		<i>R</i> -Form	<i>S</i> -Form	
<i>n</i> -Butane oxidation ^b				
AMO-Ne	14 \pm 2	23 \pm 1	77 \pm 1	54 (<i>S</i>)
pMMO-Mt	6.8 \pm 1.5	76 \pm 1	24 \pm 1	52 (<i>R</i>)
pMMO-Mc	7.9 \pm 1.4	75 \pm 1	25 \pm 1	50 (<i>R</i>)
<i>n</i> -Pentane oxidation ^b				
AMO-Ne	3.1 \pm 0.9	38 \pm 1	62 \pm 1	24 (<i>S</i>)
pMMO-Mt	3.4 \pm 1.2	86 \pm 1	14 \pm 1	72 (<i>R</i>)
pMMO-Mc	8.1 \pm 1.5	86 \pm 1	14 \pm 1	72 (<i>R</i>)

^aThe amount of 2-alcohol produced over a reaction time of 10 min. ^bThe reactions were carried out at least three times separately at 30 °C in 50 mM phosphate buffer (pH 7.0) containing 1.2 mM duroquinol, 4.5 g-wet cells per L whole cells, and *n*-butane or *n*-pentane. Initial concentration of *n*-butane and *n*-pentane dissolved in the reaction mixture was 230 μM and 92 μM , respectively. The data are shown as the average of separate reactions. ^c Defined as $|R - S|/(R + S) \times 100$, where *R* and *S* are the amount of each enantiomer. Major enantiomer is shown in parentheses.

duction of 1- and 2-pentanol indicates that the oxidation reaction is selectively proceeded at C-1 and C-2 position of *n*-pentane. The major product of the *n*-pentane oxidation was 1-pentanol; the selectivity for 1-pentanol was 74%, and the selectivity was constant during the reaction. This regioselectivity indicates that *n*-pentane oxidation proceeds predominantly when the C-1 position of *n*-pentane is located close to the catalytic site of AMO-Ne. The difference in the oxidation position for *n*-pentane versus *n*-butane suggests that the binding state of *n*-pentane in the AMO-Ne active site is different. However, 62% of the 2-pentanol produced was the *S*-enantiomer, which is consistent with the *n*-butane oxidation. Thus, AMO-Ne also has the ability to recognize the pro-*S* hydrogen at the C-2 position of *n*-pentane, although the selectivity is lower than that of *n*-butane.

To compare the ability of AMO-Ne to discriminate between the prochiral hydrogens at the C-2 position of *n*-butane and *n*-pentane with those of pMMO-Mc and pMMO-Mt, we submitted *n*-butane and *n*-pentane for oxidation with the whole cells of pMMO-Mc and pMMO-Mt. The amount of 2-alcohol produced in the reactions over 10 min and the distributions of enantiomers in the 2-alcohol are summarized in Table 1. The distributions were almost consistent with results of the previous works by us and other group.³

The amount of 2-alcohol produced was dependent on the kind of bacterial strains as shown in Table 1. In this study, we used whole cells for the reactions due to the instability of isolated enzymes *in vitro*. Possibly, morphology of bacterial cells and composition of bacterial membranes affect the access of *n*-butane and *n*-pentane to the enzymes in cells, which are not the properties of enzyme itself. Therefore, differences in the amount of 2-alcohol between the bacteria shown in Table 1 cannot be considered simply as differences in the ability between the enzymes.

On the other hand, the distribution of enantiomers in the reactions can be considered the recognition ability of enzymes.

The enantioselectivity of AMO-Ne for 2-alcohols from *n*-butane and *n*-pentane is clearly distinct from that of pMMO-Mc and pMMO-Mt. AMO-Ne predominantly produces (*S*)-2-alcohols from *n*-butane and *n*-pentane, while the two pMMOs produce (*R*)-2-alcohols selectively. The inversion of the prochiral hydrogen orientation at the C-2 position of *n*-butane and *n*-pentane is probably due to the structural difference in the substrate binding site between AMO-Ne and the two pMMOs.

2.2 Comparison of amino acid residues composing putative substrate binding cavity

In pMMO, putative cavities where the substrate could bind are located adjacent to the metal binding centers (Fig. 2).⁹ Comparison of the amino acid residues composing the surface of the cavity of the two pMMOs and AMO-Ne (Fig. 3) shows that three amino acid residues of AMO-Ne (His 141 and Ala 156 of AmoB, and Met 56 of AmoC) adjacent to the di-copper center are substituted for Trp, Ile, and Leu, respectively, in the two pMMOs. On the other hand, all of the amino acid residues composing the cavities adjacent to the mono-copper center and the tri-copper center are completely conserved for the three enzymes. Amino acid residues proximal to the substrate binding site tend to affect the ability of substrate binding more strongly than those distal from the site.¹⁶ Therefore, the distinct product selectivities for AMO-Ne and the pMMOs suggest that one or more of the amino acid residues composing the substrate binding site of AMO-Ne should be different from those of the two pMMOs, and that the amino acid residues likely affect the enzyme's ability to control the orientation of *n*-butane and *n*-pentane. Thus, according to the results of the amino acid alignment, the cavity adjacent to the di-copper center in the three enzymes is most likely the substrate binding site. The di-copper center was proposed as the catalytic site by other group based on methane oxidation activity of the recombinant pMMO subdomain containing only the di-copper center.⁶

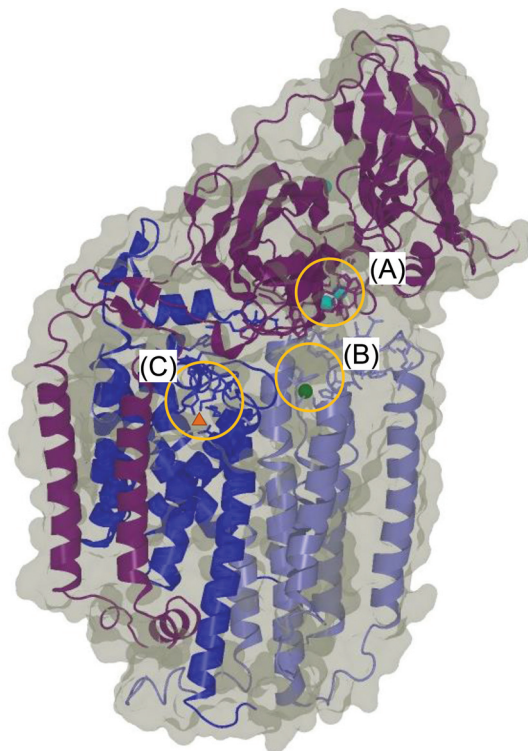


Fig. 2 Three metal binding sites in the protein structure of pMMO-Mc. (A) Di-nuclear copper site; (B) mono-nuclear copper site; (C) tri-nuclear copper site.

(A) Di-nuclear copper site

PmoC-Mc	76	A GTDSF	160	HQ T IVRD	PmoA-Mc	189	VRTGT
PmoC-Mt	49	AGLDSF	133	HM T IVRD	PmoA-Mt	194	VRTSM
AmoC-Ne	54	HGMDSM	140	HQ V IIRD	AmoA-Ne	194	VRTGT

PmoB-Mc	33	HGE	90	NV G MPGPV	134	GD W H V HTMNVQGGPIIGPGKWIT
PmoB-Mt	40	HGE	97	NAG E PGPV	141	GR W H V HAQINVEGGPIIGPGQWIE
AmoB-Ne	38	HGE	95	NV G SPSPV	139	GR B HM H AMLNVKDGPIIAGPGAWMN

(B) Mono-nuclear copper site

PmoC-Mc	75	SAGLDSFAPE F ET	154	EQDGT W HQ T IVRD T DF T PSHII
PmoC-Mt	48	RAGLDSFAPE F QT	127	EQDGT W HMT V IRD T DF T PSHII
AmoC-Ne	53	SHGMDSMEPE F DR	134	EQDAS W HQ V IIRD T S F T P SHV

(C) Tri-nuclear copper site

PmoA-Mc	36	SY H I H AM L T M GD W DF W SDWK	98	LGEWINRY
PmoA-Mt	41	GY H I H F M L T AG D W D F W VDWK	103	IGEWINRY
AmoA-Ne	41	TY H M H F M L L AG D W D F W MDWK	103	IGEWLTRY

Fig. 3 Comparison of the amino acid residues composing the cavities adjacent to the three metal binding centers in pMMO-Mc, pMMO-Mt, and AMO-Ne.

The three different colored ribbons represent the peptides composing pMMO-Mc: PmoA, PmoB, and PmoC are blue, purple, and pale purple, respectively.

The amino acid residues composing the protein cavity are indicated as bold letters, and the residues that are different

between AMO-Ne and the two pMMOs are shown by white letters on a black background.

2.3 Spatial structure of the putative substrate binding cavity

To evaluate the influence of the different amino acid residues composing the cavity's surface described in section 2.2 on the orientation of *n*-butane and *n*-pentane in the substrate binding site, protein structures of AMO-Ne and pMMO are required. However, the crystal structure of AMO-Ne has not been revealed. Therefore, we constructed a homology model of the cavity adjacent to the di-nuclear copper site of AMO-Ne (Fig. 4(B)) based on the pMMO-Mc protein structure (PDB ID: 3RGB) (Fig. 4(A)). The model was constructed by replacing the three amino acid residues (Trp136 and Ile151 of PmoB, and Ile78 of pMMO-Mc) with His, Ala, and Met, respectively.

In the cavity of pMMO-Mc, there are two pockets around the bottom indicated as *Pckt-1* and *Pckt-2* in Fig. 4(A). The spatial volume of *Pckt-2* is larger than that of *Pckt-1*. The substitution of Ile for Ala makes the volume of *Pckt-1* larger because of the difference in the van der Waals volumes of Ile and Ala (0.165 and 0.090 nm³, respectively).¹⁷ Furthermore, the substitution of Trp for His makes the entrance of the cavity wider. These structural changes are consistent with the difference in the substrate range between pMMO-Mc and AMO-Ne; AMO-Ne can oxidize larger substrates, such as aromatics, than pMMO-Mc.¹⁴ In conclusion, one or more of the three amino acid residues adjacent to the di-copper site may affect the substrate range and the selectivity for *n*-butane and *n*-pentane oxidation to alcohol isomers.

Alternatively, the amino acid residues at locations other than the surface of the putative cavity in pMMO/AMO affect catalytic selectivity. Once a method for site-directed mutagenesis of pMMO or AMO is established, the three amino acid residues mentioned above will be promising targets for changing the substrate scope, and the regio- and enantioselectivity of *n*-alkane oxidation to alcohols. In addition, construction of the model of substrate binding site in pMMO/AMO family proteins by the theoretical calculation such as QM/MM method can expect the regio- and enantioselectivity.

Copper ions are shown as blue balls, amino acid residues differing between pMMO-Mc and AMO-Ne are shown as red sticks, and the Connolly surface of the protein is shown in gray. The right side of the cavity opens up to the outside of the protein molecule.

2.4 Orientation of *n*-butane and *n*-pentane in the putative substrate binding site of AMO-Ne and pMMO-Mc

Based on the protein structure of the putative substrate binding cavity shown in Fig. 4, the proposed orientation of *n*-alkanes relative to the catalytic site is shown in Fig. 5. In the case of pMMO-Mc, (*R*)-2-alcohols are produced selectively from *n*-butane and *n*-pentane. In *n*-alkane oxidation by pMMO-Mc, proton abstraction and hydroxyl group insertion occurs with concerted mechanism.¹¹ According to this mechanism, the enantioselectivity indicates that the pro-*R* hydrogen at the C-2 position of the *n*-alkanes is predominantly located close to the

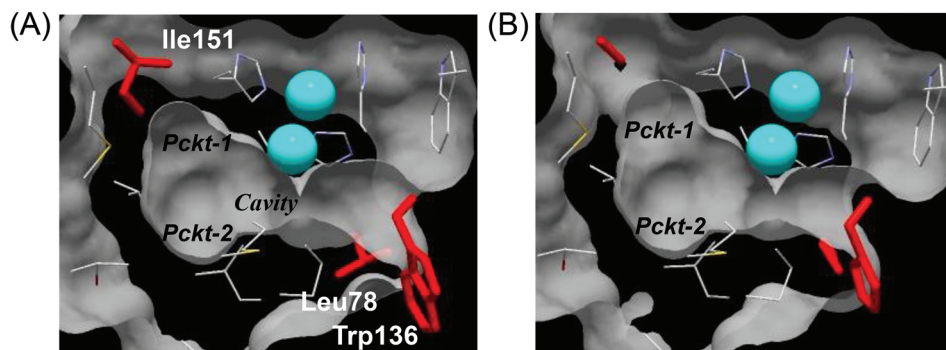


Fig. 4 Protein surface structure of the cavity adjacent to the di-nuclear copper center of pMMO-Mc and AMO-Ne. (A) Protein structure of pMMO-Mc (PDB: 3RGB). (B) Homology model structure of AMO-Ne.

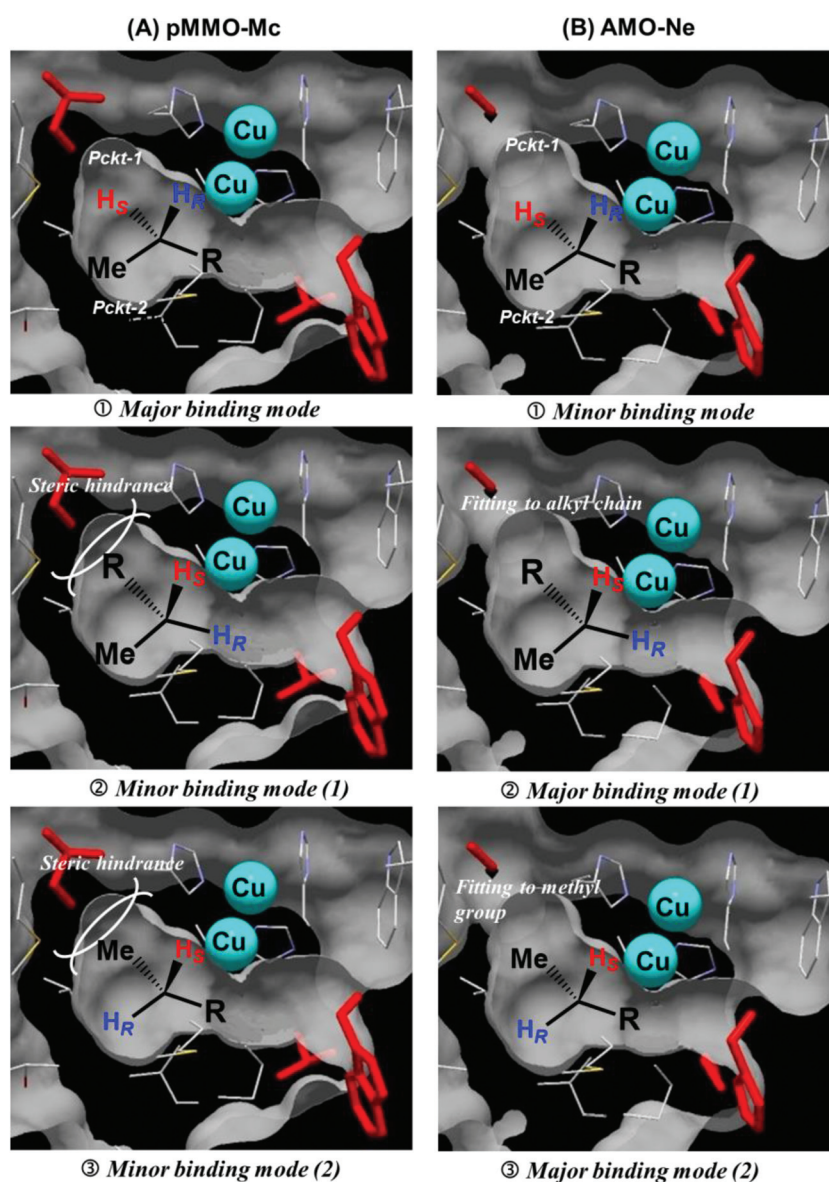


Fig. 5 Proposed orientation of *n*-butane and *n*-pentane relative to the di-nuclear copper center in the putative substrate binding cavity in pMMO-Mc (A) and AMO-Ne (B). R: Ethyl or *n*-propyl group; Me: methyl group; H_S and H_R: pro-S and pro-R hydrogens, respectively.

catalytic site in the substrate binding site of pMMO-Mc. This orientation can be explained by the model shown in Fig. 5(A)-①, where the pro-*S* hydrogen is directed toward *Pck*t-1, the methyl group is toward *Pck*t-2, and the alkyl group, such as ethyl and *n*-propyl, is toward the entrance of the cavity. Alternatively, if the pro-*S* hydrogen is oriented toward the catalytic site, then the methyl group is directed toward *Pck*t-2 and the alkyl group is directed toward *Pck*t-1 as shown in Fig. 5(A)-②, and/or the alkyl group is directed toward *Pck*t-2 and the methyl group is directed toward *Pck*t-1 as shown in Fig. 5(A)-③. However, (*S*)-2-pentanol was a minor product in *n*-pentane oxidation to 2-pentanol. Probably, the volume of *Pck*t-1 is not large enough to accommodate methyl, ethyl and *n*-propyl groups, whose molecular volumes are about 0.027 nm³, 0.044 nm³, and 0.061 nm³, respectively,¹⁸ and *Pck*t-2 is not large enough for ethyl and *n*-propyl groups. Thus, these orientations are minor conformers for the binding of *n*-butane and *n*-pentane at the catalytic site in pMMO-Mc.

As shown in Fig. 4, the protein structure of the putative substrate binding cavity in AMO-Ne is locally different from that in pMMO-Mc. The change from Ile to Ala in *Pck*t-1 increases the volume of *Pck*t-1 by about 0.075 nm³, which is estimated to be the change in the volume of the amino acid residue substituted. Therefore, *Pck*t-1 in AMO-Ne is large enough to accommodate methyl, ethyl, and *n*-propyl groups, as shown in Fig. 5(B)-② and -③. In this case, the pro-*S* hydrogen can point toward the di-copper site, which produces (*S*)-2-alcohols selectively when the oxidation reaction proceeds at the C-2 position of *n*-butane and *n*-pentane. In fact, the *S*-enantiomer was the major product when the oxidation reaction of *n*-butane and *n*-pentane proceeded at C-2 position, as described in section 2.1. This result indicates that the orientations shown in Fig. 5 (B)-② and -③ are preferable conformers for the binding of *n*-butane and *n*-pentane at the catalytic site in AMO-Ne than that in Fig. 5(B)-①. This may be caused by the optimum packing of methyl, ethyl, and *n*-propyl groups in *Pck*t-1. The molecular volumes of methyl, ethyl and *n*-propyl groups are calculated to be about 0.027 nm³, 0.044 nm³ and 0.061 nm³, respectively.¹⁸

These volumes may be optimum for packing the alkyl chains within *Pck*t-1; fitting the inner surface of *Pck*t-1 to the alkyl chains makes the conformers shown in Fig. 5(B)-② and -③ stable and favorable.

In the oxidation of *n*-butane and *n*-pentane to alcohols with AMO-Ne, the selectivity for 1-alcohols was higher than that of pMMO-Mc. This result indicates that the C-1 position of the *n*-alkane molecule is preferably positioned close to the catalytic site of AMO-Ne unlike that of pMMO-Mc. The larger space around the entrance of the cavity in AMO-Ne than that in pMMO-Mc may cause the difference in the *n*-butane and *n*-pentane orientation within the substrate binding site. Therefore, *n*-butane and *n*-pentane may bind around the entrance prior to diffusing into the cavity, resulting in orientation of the C-1 position of the *n*-alkanes close to the catalytic site.

2.5 C₆–C₈ *n*-alkane oxidation by AMO-Ne

Previous reports have indicated that AMO-Ne can oxidize larger substrates in molecular size than *n*-pentane (0.096 nm³).¹³ Thus, we submitted C₆–C₉ *n*-alkanes to the oxidation conditions using AMO-Ne whole cells to investigate the dependence of the recognition ability for the pro-*R* hydrogen at the C-2 position of *n*-alkanes on the carbon chain length. Alcohol isomers were produced from C₆–C₈ *n*-alkanes using whole cells, but not from *n*-nonane. This result suggests that the cavity size of the substrate binding site in AMO-Ne can accommodate *n*-octane (0.147 nm³), but not *n*-nonane (0.164 nm³).¹⁸

Oxidation of C₆–C₈ *n*-alkanes afforded only 1- and 2-alcohols (Fig. S1(B)–(D) in ESI†). As shown in Table 2, the distribution of 1- and 2-alcohols is dependent on the *n*-alkane, as reported previously.^{14a} 1-Hexanol was the major product from *n*-hexane, and its distribution in the product was 74%. However, for *n*-heptane the amount of 1-heptanol and 2-heptanol produced was almost the same. This result indicates that the position of the *n*-alkane molecule relative to the catalytic site is strongly influenced by the chain length of the *n*-alkane. In the case of *n*-alkane oxidation with manganese porphyrin,

Table 2 *n*-Alkane oxidation by AMO-Ne^a

Substrate ^b	Amount of alcohols ^c (μmol g-wet per cells)	Distribution of alcohol regioisomers (%)		Distribution of 2-alcohol enantiomers (%)		ee ^d (%)
		1-Alcohol	2-Alcohol	<i>R</i>	<i>S</i>	
<i>n</i> -C ₄ H ₁₀	16.5 ± 2.1	18 ± 1	82 ± 1	23 ± 1	77 ± 1	54 (<i>S</i>)
<i>n</i> -C ₅ H ₁₂	12.7 ± 2.2	74 ± 1	26 ± 1	38 ± 1	62 ± 1	24 (<i>S</i>)
<i>n</i> -C ₆ H ₁₄	13.6 ± 2.6	73 ± 1	27 ± 1	72 ± 1	28 ± 1	44 (<i>R</i>)
<i>n</i> -C ₇ H ₁₆	6.4 ± 1.8	48 ± 2	52 ± 2	83 ± 1	17 ± 1	66 (<i>R</i>)
<i>n</i> -C ₈ H ₁₈	1.8 ± 1.2	97 ± 1	5 ± 1	48 ± 1	52 ± 1	4 (<i>S</i>)

^a The reactions were carried out at least three times separately at 30 °C in 50 mM phosphate buffer (pH 7.0) containing 1.2 mM duroquinol, 4.5 g-wet cells per L whole cells, and *n*-alkane. The data are shown as the average of three separate reactions. ^b Initial concentration of substrate dissolved in the reaction mixture was: [*n*-C₄H₁₀] = 230 μM; [*n*-C₅H₁₂] = 92 μM; [*n*-C₆H₁₄] = 60 μM; [*n*-C₇H₁₆] = 38 μM; [*n*-C₈H₁₈] = 31 μM. ^c The amount of 2-alcohol produced over a reaction time of 10 min. ^d Defined as $|R - S| / (R + S) \times 100$, where *R* and *S* are the amount of each enantiomer. Major enantiomer is shown in parentheses.

the position of oxidation in the *n*-alkane can be changed by introducing bulky groups around the Mn center.¹⁹ Therefore, it is reasonable to assume that the steric hindrance caused by the amino acid residues around the catalytic site affect the position of the *n*-alkane relative to the catalytic site.

For the 2-alcohols generated from C₄–C₇ *n*-alkanes, one enantiomer was predominant; however, essentially racemic 2-octanol was produced from *n*-octane (Table 2). These distributions indicate that the ability of AMO-Ne to discriminate between the prochiral hydrogens at the C-2 position varies according to the chain length of the *n*-alkane. The enantioselectivity for (*R*)-2-alcohols increased as the chain length of the *n*-alkanes increased from four to seven. This increment is consistent with the increment in the enantioselectivities of the two pMMOs for (*R*)-2-alcohols when the *n*-alkane chain length increased from four to five, as previously discussed (see Table 1). The increment in the enantioselectivity for (*R*)-2-alcohol means that the recognition ability for C–H bond orientation at the C-2 position of the *n*-alkane gradually changed for increasing molecular size. The cavity volume of the substrate binding site in AMO-Ne may determine the C–H bond orientation of *n*-alkanes relative to the catalytic site.

By the proposed *n*-alkane orientation in AMO-Ne shown in Fig. 5(B)-②, the increment in the enantioselectivity for (*R*)-2-alcohol can be explained. The volume of *Pckt-1* (Fig. 5(B)) is approximately 0.075 nm³. This volume is enough for accommodating a propyl group (~0.061 nm³), which is the respective sidechain for oxidation of *n*-pentane at the C-2 position as shown in Fig. 6(a). However, the volume is not large enough to accommodate a butyl group (~0.078 nm³), which is the respective sidechain for oxidation at the C-2 position of *n*-hexane. Because of steric hindrance in *Pckt-1*, the *pro-R* hydrogen at the C-2 position should be oriented (Fig. 5(B)-①) as the major binding mode when the chain length of the *n*-alkane is six (Fig. 6(b)) and seven. Therefore, (*R*)-2-alcohol is the major enantiomer in *n*-hexane and *n*-heptane oxidations.

On the other hand, based on the proposed orientation shown in Fig. 5(B)-③, the alkyl group (**R**) is directed toward the entrance of the substrate binding cavity. The space around the entrance has enough space for accommodating pentyl group. According to the selectivity for 2-alcohol enantiomers, when the carbon number of the *n*-alkane increases, the orientation of *n*-alkane shown in Fig. 5(B)-③ should change to that shown in Fig. 5(B)-①. When the carbon number of the *n*-alkane increases from four to seven, *n*-alkane may not be able to enter deep enough into the cavity for interact methyl group with *Pckt-1* as shown in Fig. 6(c). In this case, the methyl group can interact with the surface of *Pckt-2* as shown in Fig. 6(b), resulting that *pro-R* hydrogen is directed toward the active site.

The hypothesis of *n*-alkane orientation within AMO-Ne cavity described above is proposed by assuming that *n*-alkane oxidation to alcohol occurs with concerted mechanism proposed as the reaction mechanism of pMMO-Mc. Therefore, after the homolytic cleavage between *pro-S* hydrogen and carbon of *n*-alkane and prior to the insertion of hydroxyl

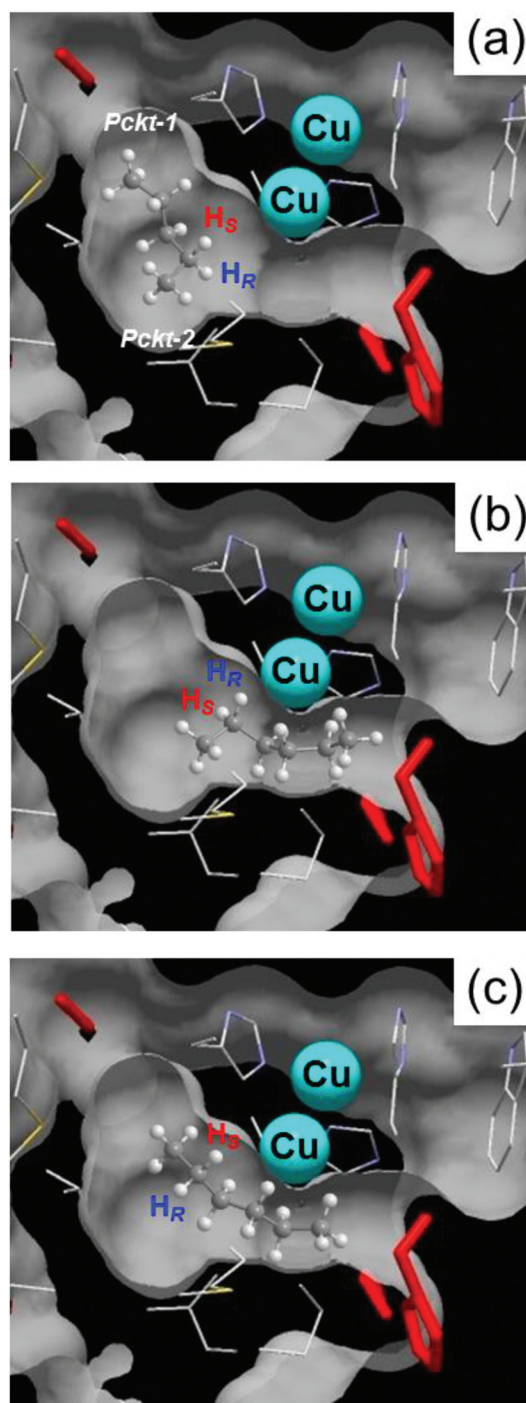


Fig. 6 Putative orientation of *n*-pentane (a) and *n*-hexane (b)(c) in the substrate binding cavity of AMO-Ne.

group, inversion of configuration at C-2 position of *n*-alkane may occur to some extent. Alternatively, *pro-R* hydrogen is abstracted from C-2 position of *n*-alkane but the hydroxyl group may be inserted from the opposite face radical intermediate. Considering these inversions, *n*-alkane orientations in the substrate binding cavity are more complicated than those shown in Fig. 5.

Table 3 *n*-Butane and *n*-pentane oxidation by AMO in whole cells of *N. europaea* with various electron donor^a

Substrate ^b	Amount of alcohols ^c (μmol g-wet per cells)	Distribution of alcohol regioisomers (%)		Distribution of 2-alcohol enantiomers (%)		ee ^d (%)
		1-Alcohol	2-Alcohol	R	S	
<i>n</i> -Butane oxidation						
Duroquinol	16.5 ± 2.4	18 ± 1	82 ± 1	23 ± 1	77 ± 1	54 (S)
NH ₄ Cl	16.9 ± 3.2	20 ± 1	80 ± 1	23 ± 1	77 ± 1	54 (S)
N ₂ H ₄	13.9 ± 2.2	21 ± 1	79 ± 1	24 ± 1	76 ± 1	52 (S)
<i>n</i> -Pentane oxidation						
Duroquinol	12.7 ± 3.2	76 ± 1	24 ± 1	38 ± 1	62 ± 1	24 (S)
NH ₄ Cl	11.7 ± 3.0	76 ± 1	24 ± 1	39 ± 1	61 ± 1	22 (S)
N ₂ H ₄	8.4 ± 2.1	71 ± 1	29 ± 1	45 ± 1	55 ± 1	10 (S)

^a The reactions were carried out at least three times separately at 30 °C in 50 mM phosphate buffer (pH 7.0) containing 1.2 mM duroquinol, 4.5 g-wet cells per L whole cells, and *n*-alkane. The data are shown as the average of three separate reactions. ^b Initial concentration of substrate dissolved in the reaction mixture was: [*n*-C₄H₁₀] = 230 μM; [*n*-C₅H₁₂] = 92 μM; [*n*-C₆H₁₄] = 60 μM; [*n*-C₇H₁₆] = 38 μM; [*n*-C₈H₁₈] = 31 μM. ^c The amount of 2-alcohol produced over a reaction time of 10 min. ^d Defined as $|R - S|/(R + S) \times 100$, where *R* and *S* are the amount of each enantiomer. Major enantiomer is shown in parentheses.

2.6 Influence of electron donor on selectivity

In the reactions described above, duroquinol was used as the electron donor for AMO-Ne. On the other hand, ammonium ions (NH₄⁺) and hydrazine (N₂H₂) can be used as alternative electron donors for AMO-Ne.^{14b} According to the molecular size of the substrates for AMO-Ne, duroquinol is too large to enter into the substrate binding site of AMO-Ne. In contrast, NH₄⁺ and N₂H₄ are similar in size to methane and ethylene, respectively, thus they can be accommodated in the substrate binding site of AMO-Ne. In the case of cytochrome P450 BM-3, co-occupation of substrate or its analogue alters product distributions.²⁰ These electron donors may be able to co-exist with *n*-alkane molecules in the substrate binding cavity, thus affecting the orientation of the *n*-alkane.

To examine the influence of the electron donors on enantioselectivity, we performed *n*-butane and *n*-pentane oxidation by AMO-Ne with NH₄Cl or N₂H₂. As shown in Table 3, almost no effect by the two electron donors was observed on the regio- and enantioselectivity for the oxidation of *n*-butane to butanol isomers. In contrast, N₂H₂ affected the selectivity of the *n*-pentane oxidation in favor of (*R*)-2-pentanol. The increased selectivity for (*R*)-2-alcohols was previously observed for longer chain lengths of *n*-alkanes (see Table 2). In conclusion, N₂H₂ may co-exist with *n*-pentane in the substrate binding cavity and affect its orientation, while NH₄⁺ may be too small to affect the orientation.

3. Conclusions

In conclusion, we have shown that the substrate binding site of AMO-Ne can discriminate between the prochiral hydrogens at the C-2 position of *n*-alkanes. The orientation of the *n*-alkane relative to the catalytic site is dependent on the *n*-alkane. Furthermore, AMO-Ne differs from pMMO-Mc and pMMO-Mt in its ability to discriminate between the size of the

n-alkane oxidized, to discriminate between the C-1 and C-2 positions, and to discriminate between the prochiral hydrogens at the C-2 position of *n*-butane and *n*-pentane. We predict that at least one of the three amino acid residues at the di-copper site affects the discriminating ability of the pMMO/AMO family proteins. Mutagenesis of the amino acid residues has the potential to invert or increase the enantioselectivity for the oxidation of *n*-alkanes to 2-alcohols. In addition, substrate analogue can also be applied for tuning the regio- and enantioselectivity of for pMMO/AMO family proteins.

4. Experimental section

4.1 Culture of bacteria

Whole cells of *N. europaea* (ATCC19718) were used for the *n*-butane, *n*-pentane, *n*-hexane, *n*-heptane, and *n*-octane oxidation reactions. The cells were grown on a 3 L scale in mineral salt medium as described previously.²¹ During culture growth, the pH of the medium was adjusted to 7.8 by the addition of 5% (w/v) Na₂CO₃. The cells were grown to logarithmic phase, and then harvested by centrifugation (12 000g for 15 min). The cells were washed with 50 mM phosphate buffer containing 2 mM MgCl₂, pH 7.7, followed by centrifugation at 12 000g for 15 min. The collected cells were suspended in 50 mM phosphate buffer containing 2 mM MgCl₂, pH 7.0, frozen in liquid nitrogen, and stored at -80 °C.

Whole cells of *M. capsulatus* (Bath) and *M. trichosporium* OB3b were also used for *n*-butane and *n*-pentane oxidation reactions. These bacteria were prepared as reported previously.^{3b}

4.2 *n*-Alkane oxidation to alcohol

n-Alkane oxidation reactions were carried out using a 50 mL 3-neck flask in a water bath at 30 °C under atmospheric pressure. The flask contained 13.5 mL of 50 mM phosphate

buffer (pH 7.0) containing 1 mM duroquinol. For the oxidation of *n*-butane, the flask was put under vacuum, and then filled with *n*-butane and air (provided by the balloons). For the oxidation of liquid *n*-alkanes, the *n*-alkane was added using a glass syringe to the buffer solution in the flask under atmospheric pressure. To initiate the reaction, bacterial cells (1.5 mL) suspended in 50 mM phosphate buffer (pH 7.0) (*ca.* 0.5 mg dry cells per mL) were added to the reactor using a glass syringe. Aliquots of the reaction mixture were withdrawn and immediately placed on ice to quench the reaction. The aliquots were centrifuged briefly to pellet the bacterial cells, then products were extracted from the supernatant using dichloromethane and analyzed by gas chromatography. The amount of product was determined using a TC-WAX column (30 m × 0.25 mm i.d., 0.25 μm film thickness, GL Science) and a flame ionization detector. The injector and detector were kept at 250 °C. The flow rate of carrier gas (He) was 34 cm min⁻¹. Temperature programs for separating each alcohol enantiomers were as follows: 40 °C for 5 min, 10 °C min⁻¹ to 230 °C.

The 2-alcohol enantiomers were identified using a method previously reported.²² The dichloromethane solutions of the 2-alcohol products previously extracted (400 μL) were dried over MgSO₄ and derivatized with trifluoroacetate (22 μL) to the corresponding esters. Enantioselectivities were determined by using a Chiraldex G-TA column (20 m × 0.25 mm i.d., 0.12 μm film thickness, Sigma-Aldrich) and a flame ionization detector. The injector and detector were kept at 250 °C. The flow rate of carrier gas (He) was 34 cm min⁻¹. Temperature programs for separating each alcohol enantiomers were as follows: 2-butanol and 2-pentanol: 30 °C for 2 min, 2 °C min⁻¹ to 170 °C; 2-hexanol and 2-heptanol: 30 °C for 2 min, 5 °C min⁻¹ to 170 °C; 2-octanol: constant at 60 °C.

The representative chromatograms of the enantiomers with their retention time in the reaction mixtures were shown in ESI (Fig. S2[†]). Retention times of each enantiomers are shown in the chromatograms. The retention times were identified by using authentic standard prepared by the reaction with trifluoroacetate with commercially available racemic 2-alcohols and either enantiomer of 2-alcohols. Racemic 2-alcohols were purchased from Kanto Chemical Co. (*S*)-2-butanol, (*R*)-2-hexanol, and (*R*)-2-octanol were obtained from Tokyo Chemical Industry Co., (*R*)-2-hexanol was from Wako Pure Chemical Industries, and (*S*)-2-heptanol was from Sigma-Aldrich. Based on the area of each peaks due to the 2-alcohol enantiomers, distribution of enantiomers was calculated.

4.3 Alignment of amino acid sequences

The amino acid sequences of the enzymes were obtained from the NCBI protein database, and multiple alignments of these sequences were performed using ClustalW.²³ A protein structure model of AMO-Ne was constructed and visualized using MolFeat ver. 4.6 (FiatLux Co., Tokyo, Japan).

Acknowledgements

This work was supported by JSPS KAKENHI Grant Number 23760739, 25630363.

References

- 1 J. A. Labinger, *J. Mol. Catal. A: Chem.*, 2004, **220**, 27–35.
- 2 K. Godula and D. Sames, *Science*, 2006, **312**, 67–72.
- 3 (a) S. J. Elliot, M. Zhu, L. Tso, H.-H. T. Nguyen, J. H.-K. Yip and S. I. Chan, *J. Am. Chem. Soc.*, 1997, **119**, 9949–9955; (b) A. Miyaji, T. Miyoshi, K. Motokura and T. Baba, *Biotechnol. Lett.*, 2011, **33**, 2241–2246.
- 4 K. J. Burrows, A. Cornish, D. Scott and I. J. Higgins, *J. Gen. Microbiol.*, 1984, **130**, 3327–3333.
- 5 (a) L. L. Lieberman and A. C. Rosenzweig, *Nature*, 2005, **434**, 177–182; (b) A. S. Hakemian, K. C. Kondapalli, J. Telser, B. M. Hzoffman, T. L. Stemmler and A. C. Rosenzweig, *Biochemistry*, 2008, **47**, 6793–6801.
- 6 (a) R. Balasubramanian, S. M. Smith, S. Rawat, L. A. Yatsunyk, T. L. Stemmler and A. C. Rosenzweig, *Nature*, 2010, **465**, 115–119; (b) R. A. Himes, K. Barnese and K. D. Karlin, *Angew. Chem., Int. Ed.*, 2010, **49**, 6714–6716; (c) S. M. Smith, R. Balasubramanian and A. C. Rosenzweig, *Methods Enzymol.*, 2011, **495**, 195–210; (d) M. A. Culpepper, G. E. Cutsail 3rd, B. M. Hoffman and A. C. Rosenzweig, *J. Am. Chem. Soc.*, 2012, **134**, 7640–7643.
- 7 (a) M. Martinho, D. W. Choi, A. A. DiSpirito, W. E. Antholine, J. D. Semrau and E. Muenck, *J. Am. Chem. Soc.*, 2007, **125**, 15783–15785; (b) E. F. Liew, D. Tong, N. V. Coleman and A. J. Holmes, *Microbiology*, 2014, **160**, 1267–1277.
- 8 S. I. Chan and S. S. Yu, *Acc. Chem. Res.*, 2008, **41**, 969–979.
- 9 R. Balasubramanian and A. C. Rosenzweig, *Acc. Chem. Res.*, 2007, **40**, 573–580.
- 10 (a) Y. Shiota and K. Yoshizawa, *Inorg. Chem.*, 2009, **48**, 838–845; (b) K. Yoshizawa, in *Copper-oxygen chemistry*, ed. K. D. Karlin and S. Itoh, John Wiley & Sons, Inc., Hoboken, NJ, USA, 2011, p. 197; (c) R. A. Himes and K. D. Karlin, *Curr. Opin. Chem. Biol.*, 2009, **13**, 119–131.
- 11 (a) B. Wilkinson, M. Zhu, N. D. Priestley, H.-H. T. Nguyen, H. Morimoto, P. G. Williams, S. I. Chan and H. G. Floss, *J. Am. Chem. Soc.*, 1996, **118**, 921–922; (b) S. S.-F. Yu, L.-Y. Wu, K. H.-C. Chen, W.-I. Luo, D.-S. Huang and S. I. Chan, *J. Biol. Chem.*, 2003, **278**, 40658–40669.
- 12 C. Bédard and R. Knowles, *Microbiol. Rev.*, 1989, **53**, 68–84.
- 13 A. J. Holmes, A. Costello, M. E. Lidstrom and J. C. Murrell, *FEMS Microbiol. Lett.*, 1995, **132**, 203–208.
- 14 (a) M. R. Hyman, I. B. Murton and D. J. Arp, *Appl. Environ. Microbiol.*, 1988, **54**, 3187–3190; (b) M. R. Hyman and P. M. Wood, *Biochem. J.*, 1983, **212**, 31–37; (c) W. K. Keener and D. J. Arp, *Appl. Environ. Microbiol.*, 1994, **60**, 1914–1920.

- 15 C. A. G. M. Weijers, C. G. van Ginkel and J. A. M. de Bont, *Enzyme Microb. Technol.*, 1988, **10**, 214–218.
- 16 S. Park, K. Morley, G. P. Horsman, M. Holmquist, K. Hult and R. J. Kazlauskas, *Chem. Biol.*, 2005, **12**, 45–54.
- 17 Y. Harpaz, M. Gerstein and C. Chothia, *Structure*, 1994, **2**, 641–649.
- 18 A. Bondi, *J. Phys. Chem.*, 1964, **68**, 441–451.
- 19 B. R. Cook, T. J. Reinert and K. S. Suslick, *J. Am. Chem. Soc.*, 1986, **108**, 7281–7286.
- 20 D. A. Rock, B. N. Perkins, J. Wahlstrom and J. P. Jones, *Arch. Biochem. Biophys.*, 2003, **416**, 9–16.
- 21 S. A. Ensign, M. R. Hyman and D. J. Arp, *J. Bacteriol.*, 1993, **175**, 1971–1980.
- 22 (a) J. H. Mommers, S. M. de Wildeman, W. A. Koolen and A. L. Duchateau, *J. Chromatogr. A*, 2008, **1182**, 215–218; (b) S. Peter, S. M. Kinne, X. Wang, R. Ullrich, G. Kayser, J. T. Groves and M. Hofrichter, *FEBS J.*, 2011, **278**, 3667–3675.
- 23 M. A. Larkin, G. Blackshields, N. P. Brown, R. Chenna, P. A. McGettigan, H. McWilliam, F. Valentin, I. M. Wallace, A. Wilm, R. Lopez, J. D. Thompson, T. J. Gibson and D. G. Higgins, *Bioinformatics*, 2007, **23**, 2947–2948.